QM/MM Modeling of Benzene Hydroxylation in Human Cytochrome P450 2C9†

Christine M. Bathelt, Adrian J. Mulholland,* and Jeremy N. Harvey*

Centre for Computational Chemistry, School of Chemistry, University of Bristol, Cantocks' Close, Bristol BS8 1TS, U.K.

Received: February 26, 2008; Revised Manuscript Received: May 30, 2008

The mechanism of benzene hydroxylation was investigated in the realistic enzyme environment of the human CYP 2C9 by using quantum mechanical/molecular mechanical (QM/MM) calculations of the whole reaction profile using the B3LYP method to describe the QM region. The calculated QM/MM barriers for addition of the active species Compound I to benzene are consistent with experimental rate constants for benzene metabolism in CYP 2E1. In contrast to gas-phase model calculations, our results suggest that competing side-on and face-on geometries of arene addition may both occur in the case of aromatic ring oxidation in cytochrome P450s. QM/MM profiles for three different rearrangement pathways of the initially formed σ-adduct, leading to formation of epoxide, ketone, and an N-protonated porphyrin species, were calculated. Our results suggest that epoxide and ketone products form with comparable ease in the face-on pathway, whereas epoxide formation is preferred in the side-on pathway. Additionally, rearrangement to the N-protonated porphyrin species was found to be competitive with side-on epoxide formation. This suggests that overall, the competition between formation of epoxide and phenol final products in P450 oxidation of aromatic substrates is quite finely balanced.

Introduction

The cytochromes P450 are a large family of heme enzymes which have a diverse set of substrate specificities and catalyze a range of biochemical transformations.[1] The most common reactions catalyzed include carbon hydroxylation, for example, the formation of an alcohol or phenol, epoxidation and N- and O-dealkylation.[2] The importance of the CYP enzymes is reflected in their presence in all forms of life, from bacteria and fungi to insects, plants, and mammals. Particular attention has been focused on human cytochromes P450 because they contribute extensively to the metabolism of xenobiotics, such as drugs, environmental pollutants, and carcinogens.[3] More than 90% of drug oxidations in man are mediated by the CYP enzymes.[4] Important issues such as bioavailability, bioactivation, toxicity, and drug−drug interactions may be associated with CYP-mediated bioconversions.

Generally, the oxidative transformation of compounds by the CYP enzymes serves to detoxify the body. Reactions, such as hydroxylation, facilitate excretion of xenobiotic molecules as they produce more water-soluble compounds. However, metabolism can also transform xenobiotics into more reactive compounds which cause toxic responses.[5] Often, xenobiotics are metabolized by the cytochromes P450 via several pathways.[6,7] For example, the potent toxic substance, aflatoxin, can be converted to many different metabolic products by CYP enzymes, and the degree of aflatoxin toxicity depends on the metabolic pathways.[7] Although metabolites arising from hydroxylation of aflatoxin are less toxic than the parent compound, double-bond epoxidation of aflatoxin produces a highly reactive epoxide that is responsible for carcinogenic effects.

Among the commonly used pharmaceutical compounds, many contain aromatic moieties. These include, for example, the anticoagulant drug warfarin,[8] several nonsteroidal anti-inflammatory drugs (flurbiprofen,[9] diclofenac,[10] and piroxicam[11]), or the anticonvulsant drug phenytoin. Furthermore, many pollutants and toxins are benzene derivatives or polyaromatic compounds.[12]

It has been observed that CYP-catalyzed oxidation of aromatic compounds gives rise to both phenolic products and arene oxides.[13,14] The simplest aromatic compound, benzene, is an environmental toxin occurring in gasoline and tobacco smoke.[15] There is evidence that metabolism of benzene by the human CYP 2E1 yields both phenol and benzene epoxide.[14,16] Conversion to phenol has been viewed as a pathway for benzene elimination. In contrast, benzene epoxide is believed to cause toxic effects by reacting with a variety of nucleophiles, including DNA, RNA, and proteins in the cell.[5] Because the toxicity of aromatic compounds often arises from CYP-catalyzed biotransformation, it is desirable to have a thorough understanding of the mechanisms involved.

The active species in all CYP-mediated reactions is generally assumed to be a high valent iron-oxo derivative of the active site heme group known as compound I.[17,18] Knowledge on this highly reactive species comes from spectroscopic studies[19] of compound I in the related chloroperoxidase and in cytochrome P450 CYP119.[20] There has also been extensive computational work on the electronic structure of this species.[18,21−24] In compound I, the iron is present in an oxidized, oxyferryl (Fe(IV)) form with a triplet spin state, and the porphyrin ring is oxidized to a π-cation radical. In its electronic ground state, compound I has two unpaired electrons located in π^* orbitals on the Fe−O moiety coupling to one unpaired electron in a π-orbital of the porphyrin ligand with approximate a_{2u} symmetry.

Although aliphatic hydroxylation has been studied intensively,[25,26,18] fewer studies have focused on the mechanism of aromatic hydroxylation. Early studies on aromatic hydroxylation concluded that arene epoxides are obligatory intermediates,[27] mainly because of the observed NIH shift,[28] the migration of hydrogen from the site of hydroxylation to the adjacent carbon.

† Part of the "Sason S. Shaik Festschrift".

* Corresponding authors. E-mail: Adrian.Mulholland@bristol.ac.uk and jeremy.harvey@bris.ac.uk.

10.1021/jp8016908 CCC: $40.75
Published on Web 08/28/2008

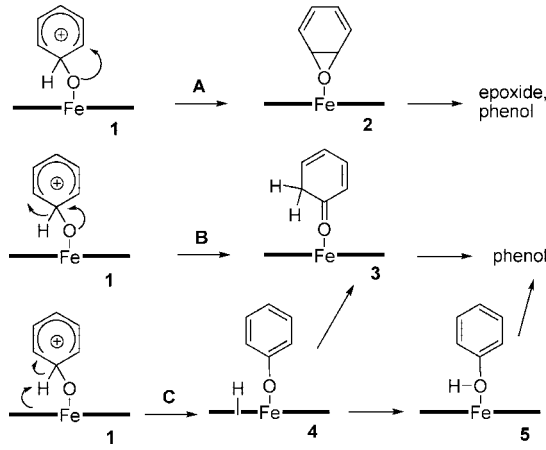

Figure 1. Rearrangement pathways from the initially formed σ-adduct between compound I and benzene, **1**. For clarity, only the cationic σ-adduct is shown. The thick line represents the plane of the heme porphyrin ring.

SCHEME 1

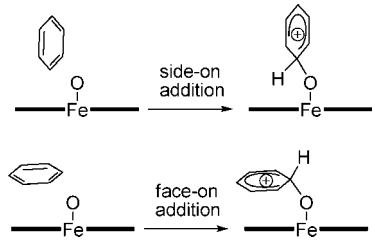

More recently, experimental evidence appeared for an alternative mechanism, the addition−rearrangement mechanism, which does not proceed via an epoxide intermediate.[29,30] It is interesting to note that experiment[31] and computation[32] suggest that similar mechanisms may be followed for the very simple compound I model species, the gas-phase FeO^+ ion. The reactivity of this ion bears many similarities to that of compound I and has played a remarkable role in developing theories of reactivity for the latter.[33]

Further evidence for the addition−rearrangement mechanism comes from computational work using larger models.[34−39] A DFT study with a model of the heme group[36] considered several alternative mechanisms for benzene hydroxylation and identified the addition−rearrangement pathway as the lowest energy mechanism. In this most likely pathway, compound I adds to a substrate carbon forming a tetrahedral intermediate σ-complex, which can be radical-like or carbocation-like. (**1** in Figure 1) All further products, phenol, ketone, and epoxide, are generated by rearrangement of these σ-complexes. DFT calculations[36−38] show that **1** can undergo competitive rearrangements to several possible species: the ferric complex of the epoxide (**2**) or of the keto tautomer of phenol (**3**, pathways A and B in Figure 1) or an N-protonated porphyrin species (**4**, pathway C). Pathway A ultimately leads to epoxides but also to phenols after nonenzymatic ring-opening of the epoxides.

Pathway B involves an NIH shift, which occurs in the initial σ-adduct. This is a common feature during the CYP-catalyzed formation of phenols.[28] It has often been observed experimentally that the substituent originally present at the carbon to be hydroxylated shifts to the adjacent carbon.[40,41] This NIH shift can also occur during nonenzymatic isomerization of the epoxide product. A further pathway (pathway C in Scheme 1) proceeds via a proton shuttle species, an N-protonated porphyrin intermediate (**4**). Computational studies by Shaik et al.[36] and results shown in our previous work[37,38] suggest that this species (**4**) could be involved in the direct formation of ketone and phenol complexes by relaying the proton from the site of attack on the aromatic carbon to the oxygen atom or the adjacent carbon.

Depending on which of the three pathways dominates, different products will be obtained from metabolism. Pathways B and C lead to products that are hydroxylated at the same carbon that was originally attacked by compound I (Scheme 1). However, pathway A yields an epoxide which can either ring open to form phenols or undergo further reactions with nucleophilic molecules (Scheme 1). Nonenzymatic ring opening of the epoxide can give two different phenolic products, one which bears a hydroxyl group at the carbon that was attacked and one that is hydroxylated at the adjacent ring carbon. For substituted aromatics, these pathways lead to different products which could have different toxicological properties. Therefore, it is desirable to gain a better understanding of the various metabolic pathways.

In our previous investigation,[37,38] we addressed general aspects of the mechanism of aromatic hydroxylation by using a small cluster model and neglecting the protein environment. It was found that addition of compound I to a substrate carbon proceeds via a transition state of mixed cationic and radical character. Moreover, an approach of benzene with its ring in a side-on orientation relative to the porphyrin ring was found to be slightly preferred over a face-on approach for oxidation of benzene itself. For some substituted benzenes, however, the preference for side-on approach disappears, and the pathways have similar barrier heights. These calculations, as the analogous work on benzene hydroxylation by Shaik et al.,[36] did not take into account the enzyme environment explicitly. The effect of the enzyme environment on the mechanism of aromatic hydroxylation was neglected or approximated by a solvent continuum model.

Recently, the crystal structures of several human CYP isoforms became available,[42−44] the first one being the drug-metabolizing CYP 2C9, followed by the CYP 2C8, 3A4, 2A6, and 2D6 isoforms. With these structures available, it is possible to include a large region of the protein explicitly in the calculation. In previous work,[23] we described the electronic structure of the active species compound I in the human CYP isoforms 2C9 and 3A4 by using a combined quantum mechanical/molecular mechanical (QM/MM) approach.[45] We applied the same QM/MM method to study the electronic structure of compound I in two related heme peroxidases,[46] and the obtained results were in very good agreement with experimental findings. Thus, it has been shown that the QM/MM method employed in our group gives reliable answers to questions related with the active species compound I.

The QM/MM method has also been used extensively to study reactivity in cytochrome P450, particularly for the C−H bond activation of camphor in bacterial P450cam.[47] To our knowledge, however, it has not been applied to studies of arene oxidation. Here, we describe for the first time a whole reaction profile for aromatic hydroxylation in the realistic enzyme environment of a human CYP isoform, specifically 2C9. The mechanism of benzene hydroxylation was reinvestigated by using the QM/MM approach. Side-on and face-on modes of benzene approach were tested as well as enzyme−substrate complexes of different conformation. Our results indicate that both approaches are possible in the enzyme environment. Furthermore, the electronic structure of the transition states, and intermediates involved, were characterized and compared with that found in model calculations in the gas phase. It will be

shown that two different electronic states play a role in the reaction profiles. Finally, all possible rearrangement pathways were considered for both side-on and face-on benzene orientations.

Computational Details

Crystal Structures. Initial structures were constructed on the basis of a crystallographic structure of CYP 2C9 obtained from the Protein Data Bank.[48] There are two slightly different X-ray structures of P450 2C9 with the PDB codes 1OG2[42] and 1R9O,[43] which are referred to as structure A and B, respectively. Differences in the two structures occur in conformationally flexible regions and in the position of the side chain of Arg 108, which reaches into the active site in P450 2C9_B but is oriented toward the surface in 2C9_A. Furthermore, in 2C9_B, the substrate flurbiprofen is bound in the active site, whereas in 2C9_A, no substrate is bound. For studying the hydroxylation of benzene, the structure 2C9_A was used. Results should not depend on the chosen X-ray structure of CYP 2C9 because benzene is relatively small and nonpolar, and therefore, steric restraints and electrostatic interactions further away from the oxygenating species compound I are not expected to play a significant role.

MD Simulations: General Settings. The CHARMM22 force field[49] and the CHARMM package version c27b2[50] were used in all MM minimizations and MD simulations. Parameters for the heme group were adjusted to the compound I state (as published previously).[23] For benzene, standard CHARMM parameters were used from the CHARMM library.

All MM minimizations were performed by using 500 steps of steepest descent (SD) and 1500 steps of adopted basis Newton−Raphson (ABNR). A 13 Å cutoff for nonbonded interactions was used for all MM energy minimizations and MD simulations. A time step of 1 fs was used in all MD simulations, and SHAKE[51] restraints were applied. For stochastic boundary simulations,[52] the system was divided into a buffer region (atoms between 21 and 25 Å from the heme iron) treated by Langevin dynamics and a reaction region (atoms in a 21 Å sphere centered on the heme iron) treated by full Newtonian molecular dynamics. Friction coefficients of 62 and 250 ps^{-1} were applied to the water oxygen atoms and the protein heavy atoms in the buffer region, respectively. Protein atoms within the buffer region were restrained harmonically to their minimized positions. The buffer restraints were dependent on the distance from the center of the system, increasing toward the boundary according to a protocol used previously.[53]

MD Simulations: System Setup. Different starting structures for the MD simulations were generated manually by placing the benzene close to the Fe−O group of compound I. Two CYP 2C9/benzene complexes were built, one with the benzene molecule in a face-on orientation to the porphyrin plane and one with benzene in a side-on orientation relative to the porphyrin plane.

Then, hydrogen atoms were added to the initial enzyme/substrate complexes, and their positions were minimized. Protonation states of histidines were assigned according to their H bonding environment. The protein was truncated to a 25 Å sphere centered on the heme iron. Charged residues at the surface were neutralized to avoid unrealistic effects due to the protein truncation and insufficient screening of charges by the solvent. Glutamate and aspartate residues near the surface were protonated to neutralize the negative charge. To obtain a neutral charge for lysine and arginine residues near the surface, patch residues of the same geometry but scaled partial atom charges were used. This resulted in a net charge of 0 for CYP 2C9. The structures were solvated within a sphere with a radius of 26 Å centered on the heme iron by using pre-equilibrated water molecules, represented by the TIP3[54] model. The added water was then equilibrated by stochastic boundary MD at 310 K over 25 ps with respect to the substrate-bound enzyme structure and minimized. Water molecules further away than 25 Å from the heme iron were removed. Then, all atoms were minimized, followed by stochastic boundary MD simulation of the whole system. All systems were heated to 310 K over 50 ps. Subsequent MD equilibrations at 310 K were carried out over 100 ps. All MD simulation were performed with harmonic restraints (force constant $k = 200$ kcal/mol, $d = 2.5$ Å) on the distance between the reacting carbon and the ferryl oxygen of the heme group.

QM/MM Calculations. Starting structures were taken from the MD simulations described above. For profiles 1 of face-on and side-on benzene orientations, MM minimized snapshots after the full MD simulations were used. For profiles 2, an MM minimized snapshot after 23.5 and 83.1 ps was chosen, after visual inspection of the trajectories, for the face-on and side-on orientation of benzene, respectively.

The QM region comprised the heme group without substituents on the porphyrin ring, the SCH_2 group of the cysteinyl ligand, and the benzene molecule. The Jaguar 4.0 software[55] was used with the standard UB3LYP density functional. The open shell $^2A_{2u}$ state of compound I was generated in all calculations. This was achieved by providing an initial guess wave function constructed in the following way. First, appropriate charges and spins were assigned to molecular fragments (Fe, O, SMe, and the porphyrin ring) of the model compound, and the wave function for the quartet A_{2u} state was converged by using a restricted open-shell (ROB3LYP) ansatz. Then, the order of the obtained orbitals was rearranged, and this set of modified orbitals served as an initial guess wave function for the unrestricted $^2A_{2u}$ state. Only reactions from the doublet state of compound I were considered because it was shown, in our previous paper on aromatic hydroxylation in the gas phase,[38] that reactions starting from the $^4A_{2u}$ state lead to higher activation barriers. The standard Los Alamos effective core potential and the associated double-ζ basis LACVP[56] were used on iron, and the 6-31G basis was used on all other atoms. This combination is referred to as BSI. Results from our previous work on a small gas-phase model are given for comparison. These calculations were carried out by using BSII: the standard Los Alamos core potential and the associated triple-ζ contraction of the LACVP basis, as implemented in Jaguar, on Fe (LACV3P), and the 6-31G(d) basis on all other atoms.

The TINKER MM code[57] with the CHARMM27 all atom force field[58] was used for the treatment of the MM part of the system. Potential energy terms were computed for atoms within a sphere of 20 Å centered on the heme iron. Atoms beyond this distance were fixed.

Input and output from the Jaguar and Tinker codes were coupled by using our own set of routines (QoMMMa),[59] which was also used to optimize the geometry of the QM subset of the atoms. MM atoms were optimized at each QM step within the Tinker code. Polarization effects on the QM atoms are accounted for by including the fixed MM charges in the QM Hamiltonian. The steric QM/MM interactions are described by using van der Waals radii for the QM atoms which are taken from the CHARMM27 force field values for similar atoms. The valences of the covalent bonds at the QM/MM boundary were satisfied by using hydrogen link atoms.[60] As the other QM atoms, these additional hydrogen capping atoms are exposed

to the electric field of the MM point charges. However, MM charges on the atom replaced by the link atom, as well as those on atoms directly bonded to this atom, were set to zero to avoid nonphysical effects.

Adiabatic mapping was carried out by performing several QM/MM geometry optimizations with harmonic restraints ($k = 500$ kcal/mol) on the reaction coordinate. The following reaction coordinates were used: (i) the distance between the reacting carbon and the ferryl oxygen, for addition of benzene to compound I, (ii) the distance between one of the carbon atoms adjacent to the site of initial attack and the ferryl oxygen, for epoxide formation, (iii) the distance between the hydrogen atom on the site of attack and one of the carbon atoms adjacent to the site of attack, for the NIH shift, and (iv) the distance between the hydrogen atom at the site of attack and the nearest porphyrin nitrogen atom, for formation of the proton shuttle species. It should be noted that these are approximate reaction coordinates and will not give the exact transition state.

Reactant and product complexes were minimized without any restraints in all profiles.

Results and Discussion

Hydroxylation of the simplest aromatic compound, benzene, by the human CYP 2C9 was investigated to address general features of the reaction and determine the effects of the enzyme environment. Our aim is to get insight into how aromatic substrates in general are oxidized by human P450 isoforms, and we use the combination of benzene and CYP 2C9 as a generic model rather than as a specific case with direct biochemical relevance. Indeed, benzene itself is not metabolized by CYP 2C9. However, it is a substrate for the closely related human CYP 2E1, and its metabolites play a role in benzene toxicity.[5,16] Because there is no X-ray structure available of the CYP 2E1 isoform (there is however a homology model[61]), it is not straightforward to model benzene metabolism in that isoform. By studying the closely related CYP 2C9, we get insight into the general aspects of aromatic oxidation in P450 enzymes but cannot, of course, reach specific biochemical conclusions. For example, because benzene is a small molecule, orientational effects in the CYP 2C9 active site, which accommodates larger substrates, should not be considerable, but this will probably not be the case for other, larger, substrates. Conversely, CYP 2E1 tends to oxidize small nonpolar substrates, and some of the geometries and reaction paths optimized in the present study for CYP 2C9 may not be sterically possible in CYP 2E1. Nevertheless, the benzene/CYP 2C9 system represents a good model for studying the general characteristics of aromatic hydroxylation.

Addition of Compound I. QM/MM energy profiles were calculated for addition of the active species (compound I) to benzene. Previous QM and QM/MM studies[21−24] as well as experimental work[19] have shown that the electronic ground state of compound I is a pair of doublet and quartet A_{2u} states, with two unpaired electrons residing on the iron-oxo moiety and a third unpaired electron located on the porphyrin and to some extent on the axial sulfur ligand. Only the doublet state was considered here, because profiles starting from compound I in its quartet state gave considerably higher barriers in previous gas-phase model calculations.[36,38]

Our previous calculations[38] also showed that benzene can approach compound I in two different orientations, with its benzene ring perpendicular (side-on) or parallel (face-on) relative to the porphyrin ring (Scheme 1). There, it was found that the side-on mode of approach gives lower reaction barriers, and it was therefore predicted to be more favorable. However, steric restraints in the active site cavity may lead to different preferences in the approach of benzene to the compound I species. This is considered in the more realistic model, presented here, which includes large parts of the enzyme environment. To reinvestigate the geometry of benzene approach in the environment of the enzyme, the two different orientations of benzene were modeled in the present QM/MM study.

TABLE 1: QM/MM Activation Barriers [kcal/mol] for Addition of Compound I to Benzene for Side-On and Face-On Orientation and Activation Barrier for the Lowest Addition Profile in the Small Gas-Phase Model, C−O Distances [Å] at the TS, QM/MM Reaction Energies ΔE [kcal/mol], and Angle ϕ [degree] between the Porphyrin Plane and the Benzene Ring Plane at the TS

	barrier	d(C−O) at TS	ΔE	ϕ
side-on 1	18.1	1.79	13.02	112.1
side-on 2	21.7	1.83	14.42	94.8
side-on (gas)[a]	16.5	1.89	8.2[b]/6.9[c]	118.0
face-on 1	19.5	1.75	14.06	173.6
face-on 2	20.7	1.80	17.17	175.9
face-on (gas)[a]	19.1	1.84	4.5[b]/9.6[c]	178.6

[a] Calculated with the larger basis set BSII. [b] Cationic adduct. [c] Radical adduct.

The initial enzyme−substrate complexes were generated manually on the basis of the knowledge of the geometry for the two modes of approach observed for the small model in the gas phase.[38] It is possible that an automatic docking tool could have produced alternative starting conformations not considered by the manual docking approach. However, most likely, docking would have favored a position of the benzene molecule in the active site which allows π-stacking interactions with the aromatic ring of a Phe residue. In CYP 2C9, Phe 114 reaches into the active site and has been postulated to provide hydrophobic interactions with large aromatic substrates such as diclofenac and sulfaphenazole.[62] If benzene were to interact with this Phe 114 residue, however, it would be in a position too far away from the heme oxygen to react or serve as a reasonable starting structure for a reaction profile calculation. Furthermore, the active site pocket of CYP 2C9 is generally quite spacious but is funnel-shaped toward the heme group. Even for the small benzene molecule, the cavity becomes relatively narrow close to the heme because a number of residues, namely, Leu 366, Val 113, Leu 362, Thr 301, and Ala 297, surround the heme oxygen and restrict substrate access. Therefore, it is likely that docking algorithms would place benzene in a sterically less restricted portion of the active site cavity. To obtain a starting structure of the CYP 2C9/benzene complex for QM/MM modeling with (i) the benzene in a reactive position close to the heme and (ii) allowing favorable interactions with the protein within these limits, the following approach was used: the two manually built CYP 2C9/benzene complexes for side-on and face-on orientation were equilibrated by an MD simulation with restraints on the distance between the ferryl oxygen and the reacting carbon of the benzene molecule so as to keep benzene in a reactive position. From each of these MD trajectories (side-on and face-on), two different minimized snapshots were chosen as starting structures for calculating the QM/MM reaction profiles for side-on and face-on benzene approach. The starting structures from different MD snapshots show slight differences in the angle ϕ between the porphyrin plane and the plane of the benzene ring (side-on 1 and 2 and face-on 1 and 2, respectively, Table 1) and small conformational differences in the enzyme structure.

These QM/MM energy profiles yielded barriers between 18.1 and 21.7 kcal/mol for the addition step of benzene hydroxylation. There is some variation in barrier height between profiles 1 and 2 in each case, which differ in the starting structures (Table 1). On the other hand, there is no significant difference between the barriers to the side-on and face-on additions, at least on the basis of the small sample of barriers considered here. In contrast, previous calculations of benzene hydroxylation in the gas phase showed a clear preference for the side-on geometry of benzene.[36,38] It is appropriate to repeat here that CYP 2C9 does not oxidize benzene, and for the biochemically relevant oxidation of benzene in CYP 2E1, it is possible that the rather small active site may lead to a preference for side-on approach. But the present QM/MM calculations do suggest that for a given substrate, the enzyme environment can tune the geometry preferences derived from the gas-phase model. This suggests that, depending on the specific substrate and the shape of the active site, both side-on and face-on approach of aromatic moieties may be possible in P450 enzymes. In general, the QM/MM barriers found in the enzyme are slightly higher than those found in our previous gas-phase calculations but still comparable. The gas-phase calculations gave a barrier of 16.5 kcal/mol for the side-on pathway for benzene addition (Table 1, obtained with a larger basis set BSII; however, single-point calculations with the smaller basis set BSI used in the present QM/MM calculations gave a very similar value of 16.4 kcal/mol).

The calculated barrier heights do not include a correction for zero-point energy, which is expected to be fairly modest for most of the steps. It should also be noted that the calculated reaction barriers do not correspond to differences in free energy because they do not include contributions from entropy changes. However, the entropy difference between reactants and transition state is not expected to be large because there are no major rearrangements during the addition of compound I to benzene, and the benzene substrate will not have extensive rotational or translational entropy within the active site. Experimental rate constants[16] for hydroxylation of benzene in cytochrome P450 2E1 correspond to activation free energies of 18.8−19.4 kcal/mol when the Eyring equation at room temperature is applied. By assuming that entropy effects are not large, this is consistent with the lowest calculated QM/MM barrier heights of 18.1 and 19.5 kcal/mol for side-on and face-on hydroxylation of benzene, respectively.

Because the transition state determines the reaction barrier, it is important to characterize its properties. In the QM/MM profiles, the transition states occur slightly later, at C−O distances between 1.79 and 1.83 Å (Table 1), compared with a C−O distance of 1.89 Å at the transition state in the lowest gas-phase profile. This can be expected from Hammond's postulate[63] which relates the nature of the transition state to its location on the reaction path. In the gas phase, the energy of the formed σ-adducts for benzene was only 6.9 and 8.2 kcal/mol (BSII) above the separated reactants, for the two possible σ-adducts respectively (Table 1).[37,38] By contrast, the adducts in the enzyme lie between 13.02 and 17.17 kcal/mol (BSI) above the reactants. The formation of the σ-adduct is more endothermic in the enzyme, and according to Hammond's postulate, the transition state, in this case, resembles more closely the high-energy σ-adduct intermediate, which has a shorter C−O distance. The reasons for the higher energy of the σ-adducts in the enzyme are not clear. It might be due to the restricted space close to the heme group, which the benzene molecule needs to enter slightly more deeply when forming the σ-adduct. These steric interactions may lead to a higher energy for the formed σ-adduct compared with the gas phase where benzene is completely free to assume the most favorable conformation.

TABLE 2: Mulliken Spin (ρ_{benz})[a] and Charge (Q_{benz}) Densities on the Benzene Ring at the Transition States and in the Adducts for Addition of Compound I to Benzene in CYP 2C9 for Side-On and Face-On Pathways[b]

	$\rho_{benz}(Q_{benz})$ TS	$\rho_{benz}(Q_{benz})$ adduct
side-on 1	0.34 (0.30)	0.60 (0.43)
side-on 2	0.22 (0.39)	0.40 (0.57)
side-on (model)	−0.42 (0.34)	−0.01 (0.72)[c]/−0.86 (0.33)[d]
face-on 1	0.23 (0.29)	0.41 (0.44)
face-on 2	−0.49 (0.32)	−0.84 (0.34)

[a] The negative sign indicates excess β spin density. [b] Values for the small gas-phase model are shown for comparison. [c] Cationic adduct. [d] Radical adduct.

SCHEME 2: Schematic Representation of the Electronic Motion between the Reactants (Compound I and Benzene) and the Cationic σ-Adduct

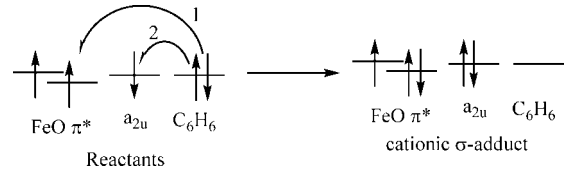

The overall characteristics of a mixed cationic and radical species at the transition state found in the gas phase are confirmed by the QM/MM calculations in CYP 2C9. However, the exact identity of the spin states involved differs. In the doublet state of compound I in both the QM model and QM/MM enzyme calculations, there are three unpaired electrons.[18] Two spin-up (or α) electrons are located in π^* orbitals on the ferryl moiety, and one spin-down (or β) electron is located in a π orbital on the porphyrin ring, of approximately a_{2u} symmetry. In the gas-phase model calculations described previously,[37,38] there remains significant α spin density on the ferryl moiety in the addition TS to benzene, and there is some β spin density on the benzene. In the QM/MM calculations, for both side-on profiles and for profile 1 of the face-on pathway, there is instead partial α spin density on the benzene at the transition state (Table 2). In both cases, formation of the cationic σ adduct requires two electrons from benzene to undergo formal transfer to compound I. One of these formally goes to one of the ferryl π^* orbitals (shown as process 1 in Scheme 2). The other is formally transferred to the porphyrin a_{2u} orbital (process 2 in Scheme 2). Note that in some cases, radical-like adducts can also be formed in which there is still some unpaired electron spin on the benzene in the adduct. In the gas-phase model TSs, where extensive β density is found on the benzene at the TS, it appears that process 1 is less advanced than process 2 at the TS, and this is reversed in the QM/MM TSs.

It is likely that the balance between which of the two formal electron transfer processes occurs first is quite easily displaced in one direction or the other depending on the environment. Indeed, for the two QM/MM pathways starting from a face-on approach of the benzene (profile 2), the observed electronic configuration at the TS is much more similar to that of the gas-phase TSs. These different electronic configurations at the TSs are summarized in Table 2, where spin densities in the QM/MM optimized σ-adducts are also shown. It can be noted that the QM/MM adducts are more radical-like that cation-like with respect to the benzene ring, because there is still considerable

TABLE 3: QM/MM Activation Barriers [kcal/mol] (BSI) Relative to the Compound I/Benzene σ-Adducts for Rearrangement to the Ketone and Epoxide Complexes for Side-On and Face-On Pathways and for the Formation of the N-Protonated Porphyrin Species for the Side-On Pathway in CYP 2C9[a]

	side-on 1	side-on 2	side-on (gas)	face-on 1	face-on 2	face-on (gas)
epoxide	1.2	4.5	0.4[b]	6.3	5.3	7.7
ketone	8.9	3.4	—[c]	5.7	5.1	0.9
shuttle	4. 9	1.4	—[c]	—[d]	—[d]	—[d]

[a] Values for the small gas-phase model (BSII) are shown for comparison. [b] From cationic σ-adduct. [c] Barrierless formation of shuttle species. [d] Pathway not possible.

unpaired electron density on benzene. In the gas phase, it was possible to separately optimize radical and cationic σ-adducts, but this was not possible in the QM/MM calculations.

In summary, the addition of benzene to compound I in CYP 2C9 gave QM/MM barrier heights between 18.0 and 21.7 kcal/mol. These values are consistent with experimental rate constants for hydroxylation of benzene in human CYP 2E1. Slight differences in the barrier heights were found for side-on and face-on approach. However, the variations due to different starting conformations do not allow for determination of a clear preference for the side-on or face-on pathway. This is in contrast to findings in the gas phase which indicate that the side-on pathway is slightly more favorable. Thus, it appears that for some substrate/CYP isoform combinations at least, both side-on and face-on pathways are possible. Furthermore, two different electronic configurations are involved in the addition of Compound I to benzene in the enzyme, and, unlike in the gas-phase model, the formed compound I/benzene σ-adducts show mixed radical and cationic character.

Rearrangement Pathways. In the previous section, the first step in aromatic hydroxylation was addressed, which leads to σ-adduct intermediates. These adducts can rearrange to final products in various ways (Scheme 1). The compound I/benzene σ-adduct structures resulting from profiles 1 and 2 of face-on and side-on pathways, respectively, were taken as a starting point. QM/MM profiles for possible rearrangements to the epoxide or ketone complexes were calculated for both pathways in the CYP 2C9 enzyme. In addition, formation of an N-protonated porphyrin complex, which was suggested to play a role as a proton shuttle,[36] was investigated for the side-on pathway.

Rearrangements to Benzene Epoxide. In the gas-phase model used in our previous DFT study,[38] epoxide formation was found to have a considerable barrier in the face-on pathway (7.7 kcal/mol), whereas epoxide formation from the cationic σ-adduct in the side-on pathway had a very low barrier (0.4 kcal/mol, Table 3). In these calculations, rearrangements from the cationic and the radical σ-adducts were considered separately. The QM/MM calculations, in the enzyme, could only generate σ-adducts with mixed radical and cationic properties, and rearrangements from these adducts were studied.

For the side-on adduct in QM/MM profile 1, ring closure to the epoxide has a very low barrier of 1.2 kcal/mol (side-on 1, Table 3), which is consistent with the findings for the gas-phase model. The higher barrier for side-on profile 2 (Table 3) might be due to the fact that formation of the metal-bound epoxide does not occur, presumably for steric reasons, and the epoxide thereby starts to dissociate from Fe along the reaction coordinate. Both barriers, however, are relatively low and suggest that epoxide formation can proceed rapidly in the enzyme.

The face-on σ-adduct, for both starting conformations, rearranges with barriers noticeably higher than those for side-on epoxidation (face-on 1 and 2 in Table 3). Although there are variations between profiles 1 and 2, in each pathway, the results indicate that side-on epoxide formation is easier than face-on epoxidation. This is in qualitative agreement with the findings for the gas-phase model from our previous study; however, the difference in the barriers to epoxide formation between the side-on and face-on pathways is smaller in the enzyme. In the-gas phase, epoxide formation from the cationic σ-adduct in the side-on pathway was found to be more favorable, by as much as 7.3 kcal/mol, compared with the face-on pathway (Table 3). By contrast, in the enzyme, the difference in barrier height between the lowest side-on epoxide formation (side-on 1) and the lowest face-on epoxidation (face-on 1) is only 4.1 kcal/mol (Table 3).

Rearrangements to Ketone and Phenol. Phenol products can form enzymatically in two ways: (i) via the formation of the keto tautomer of phenol from the initial σ-adduct of benzene with compound I and (ii) via the N-protonated porphyrin intermediate which serves as a proton shuttle (Scheme 1). Both possibilities were addressed by calculating QM/MM reaction profiles for the rearrangements.

Direct ketone formation, (i), can proceed via a 1,2 hydride shift from the compound I/benzene adduct. In the gas-phase model, this pathway could only be calculated for the face-on benzene approach. With the benzene in side-on orientation with respect to the porphyrin ligand, the ipso C−H group is in close proximity to one of the porphyrin nitrogens. Therefore, the attempt[38] to create a side-on reaction profile for 1,2 hydride shift led to instantaneous proton transfer, as was also observed by Shaik et al.[36] In the enzyme, by contrast, the 1,2 hydride shift could also be studied for the side-on approach. This might be due to a less ideal geometry for abstraction of the ipso H making this pathway less favorable and thus allowing the alternative 1,2 hydride shift.

For the face-on orientation, QM/MM barrier heights for the 1,2 hydride shift are of similar magnitude to those found for epoxide formation. This suggests that both the face-on epoxide and face-on ketone formation can occur in the enzyme (Table 3). By contrast, our previous gas-phase model calculations indicated that face-on ketone formation is considerably more favorable than face-on epoxide formation.

For the side-on pathway, QM/MM profiles for the 1,2 hydride shift led to one very high barrier of 8.9 kcal/mol (side-on 1, Table 3) and to a smaller barrier of 3.4 kcal/mol (side-on 2, Table 3). Both activation barriers, however, are higher than that for side-on epoxide formation in profile 1 (1.1 kcal/mol). It therefore appears that epoxide formation is the most favorable side-on rearrangement.

For the side-on pathway, a further rearrangement type from the σ-adduct to the N-protonated porphyrin species, which cannot occur in the face-on benzene orientation, was studied. In this rearrangement, the hydrogen atom at the tetrahedral carbon is abstracted by one of the porphyrin nitrogens (Scheme 1). Two different barrier heights were obtained from the QM/MM reaction profiles. The lower one (1.4 kcal/mol) can compete with the very small barrier of 1.1 kcal/mol (side-on 1, Table 3) found for epoxide formation. Even the higher value for the reaction barrier (4.9 kcal/mol) is not considerably higher than that for epoxide formation (4.5 kcal/mol, side-on 2, Table 3). Thus, the results indicate that the proton shuttle occurs with similar ease to epoxide formation in the side-on pathway. At some points along the reaction profile, QM/MM optimization

TABLE 4: QM/MM Energies [kcal/mol] (BSI) Relative to the Reactant Complex for Different Side-On and Face-On Pathways in CYP 2C9

	E (TS add)	*E* (adduct)	*E* (TSrearr)
side-on 1 epoxide	18.1	13.0	14.2
ketone	18.1	13.0	21.9
shuttle	18.1	13.0	17.9
side-on 2 epoxide	21.7	14.4	18.9
ketone	21.7	14.4	17.8
shuttle	21.7	14.4	15.8
face-on 1 epoxide	19.5	14.1	20.4
ketone	19.5	14.1	19.8
face-on 2 epoxide	20.7	17.2	22.5
ketone	20.7	17.2	22.3

led to the phenol complex of the ferric group. The proton, in these cases, was transferred to the oxygen atom during geometry optimization. This is in agreement with the postulated function of the N-protonated porphyrin species as a proton shuttle to produce phenol products directly.[36]

In summary, QM/MM calculations predict rearrangements to the epoxide and ketone product to occur over relatively low barriers, so that evolution to final products should be fairly rapid once the first step, the formation of the σ-adduct, has taken place. The competing rearrangements have very similar barriers in the case of face-on addition, which indicates that both epoxide and phenol products may be formed in the enzyme. In the side-on structures, reaction barriers for the different rearrangements and for different starting structures were more variable. The lowest barriers were found for epoxide formation and formation of the N-protonated porphyrin species. The NIH shift to the ketone complex seems to be less favorable in the side-on pathway, compared with formation of epoxide and shuttle species. Comparing both side-on and face-on path energies, the lowest activation barriers were found for side-on epoxide and side-on proton shuttle formation. In general, differences between the ease of different rearrangements were found to be less distinct in the QM/MM calculations compared with the findings from gas-phase model calculations. This suggests that several rearrangement pathways may occur in the enzyme. It is also possible that the preferred pathway varies for a given isoform of cytochrome P450 and a given aromatic substrate.

Overall Reaction Barriers. So far, we discussed the first reaction step, the addition of compound I, and the second reaction step, the various types of rearrangements, separately. In the gas-phase model calculations, addition of compound I was the step with the highest reaction barrier, and the subsequent rearrangements from the formed σ-adducts did not contribute to the overall barrier height. In the CYP2C9 model, however, the σ-adducts are relatively high in energy, and rearrangements from there lead to a slightly increased overall reaction barrier, in some cases. Table 4 shows combined QM/MM energies for addition and rearrangement steps for all side-on and face-on reaction pathways. In the side-on profiles, the rearrangements do not affect the overall reaction barrier. There is a high rearrangement barrier from the σ-adduct to the ketone in once case, but the other rearrangements of the same adduct proceed with low barriers. By contrast, the rearrangements to epoxide and ketone in the face-on pathway proceed over barriers that are calculated to be slightly higher than that for initial addition of compound I. In principle, then, it would appear that addition of compound I to form the σ-adduct should be reversible at least in some cases, with the rearrangement step becoming rate-limiting. However, given the limited sampling of QM/MM pathways, the uncertainties in the accuracy of the underlying B3LYP calculations, and the small difference between the barriers for the two steps, one cannot exclude the possibility that addition is always rate-limiting (as found in the model gas-phase calculations).

Conclusions

The mechanism of aromatic hydroxylation was investigated for benzene hydroxylation in a realistic enzyme environment, by using MD simulations and, for the first time, QM/MM calculations of the whole reaction profile. Benzene hydroxylation was studied in the active site of the human CYP isoform 2C9, which belongs to the same family as the CYP isoform 2E1, the natural catalyst of benzene metabolism in humans. QM/MM profiles for the addition of compound I to benzene and for three different subsequent rearrangement pathways were calculated. Different starting structures obtained from MD simulations and different orientations of benzene approach, side-on and face-on relative to the porphyrin plane, were considered for both addition and rearrangement reactions.

The obtained QM/MM barriers for the addition step of benzene hydroxylation are comparable with experimental rate constants for benzene metabolism in CYP 2E1 and thus represent realistic values. Unlike in previous DFT model calculations, side-on and face-on pathways led to comparable barrier heights for addition of compound I. Thus, our results suggest that both side-on and face-on approach of the arene ring might be able to occur in some cases of cytochrome P450 oxidation of aromatic substrates. Furthermore, it was found that two different electronic configurations, one with excess α and one with excess β spin density on the benzene, can be involved in the reaction. In general, the QM/MM profiles show more electronic and geometric variability as compared to the gas-phase calculations.

Possible rearrangements from the formed compound I/benzene σ-adducts to the epoxide and phenol (via the keto tautomer of phenol or the N-protonated porpyrin species) were studied. In the face-on pathway, formation of epoxide and ketone products was found to lead to very similar activation barriers between 5.1 and 6.3 kcal/mol relative to the σ-adducts. This suggests that both epoxide and ketone products can arise from benzene hydroxylation with face-on geometry. For the side-on orientation of benzene, reaction barriers were more variable ranging from 1.2 to 8.9 kcal/mol, depending on the rearrangement type and the starting conformation. The results indicate that, unlike in the face-on pathway, epoxide formation is more favorable than ketone formation here. Additionally, rearrangement to the N-protonated porphyrin species is possible in the side-on pathway. This rearrangement leads to low reaction barrriers competitive with those for epoxide formation. Furthermore, it was found that during this rearrangement, a phenol complex forms spontaneously during geometry optimization at certain points along the reaction path. This confirms the previously proposed role of this N-protonated species as a proton shuttle.

In conclusion, this QM/MM study shows that aromatic hydroxylation may proceed via several pathways in an enzyme environment. Both side-on and face-on pathways, different electronic state,s and various rearrangements seem possible. It is conceivable that depending on the substrate and active site geometry, products from aromatic hydroxylation are formed via all these pathways.

Note Added after ASAP Publication. The article posted ASAP on August 28, 2008. A technical error caused several

citations to be numbered incorrectly throughout the text. The correct version posted on November 12, 2008.

References and Notes

(1) Ortiz de Montellano, P. R. *Cytochrome P450. Structure, Mechanism and Biochemistry*; 3rd ed.; Plenum: New York, 2005.

(2) Guengerich, F. P. *Chem. Rev. Toxicol.* **2001**, *14*, 611.

(3) Anzenbacher, P.; Anzenbacherova, E. *Cell. Mol. Life Sci.* **2001**, *58*, 737.

(4) Lewis, D. F. *Pharmacogenomics* **2003**, *4*, 387.

(5) Snyder, R. *Drug Metab. Rev.* **2004**, *36*, 531.

(6) Lau, S. S.; Abrams, G. D.; Zannoni, V. G. *J. Pharmacol. Exp. Ther.* **1980**, *214*, 703.

(7) Eaton, D. L.; Gallagher, E. P. *Annu. Rev. Pharmacol. Toxicol.* **1994**, *34*, 135.

(8) Rettie, A. E.; Korzekwa, K. R.; Kunze, K. L.; Lawrence, R. F.; Eddy, A. C.; Aoyama, T.; Gelboin, H. V.; Gonzalez, F. J.; Trager, W. F. *Chem. Res. Toxicol.* **1992**, *5*, 54.

(9) Tracy, T. S.; Marra, C.; Wrighton, S. A.; Gonzalez, F. J.; Korzekwa, K. R. *Biochem. Pharmacol.* **1996**, *52*, 1305.

(10) Mancy, A.; Antignac, M.; Minoletti, C.; Dijols, S.; Mouries, V.; Duong, N. T.; Battioni, P.; Dansette, P. M.; Mansuy, D. *Biochemistry* **1999**, *38*, 14264.

(11) Ogiso, T.; Iwaki, M.; Tanaka, H.; Kobayashi, E.; Tanino, T.; Sawada, A.; Uno, S. *Biol. Pharm. Bull.* **1999**, *22*, 191.

(12) Guengerich, F. P. *Chem. Res. Toxicol.* **1991**, *4*, 391.

(13) Jerina, D. M.; Daly, J. W.; Witkop, B.; Zaltzman-Nirenberg, P.; Udenfriend, S. *Biochemistry* **1970**, *9*, 147.

(14) Lovern, M. R.; Turner, M. J.; Meyer, M.; Kedderis, G. L.; Bechtold, W. E.; Schlosser, P. M. *Carcinogenesis* **1997**, *18*, 1695.

(15) Sheets, P.; Carlson, G. *J. Toxicol. Environ. Health A* **2004**, *67*, 421.

(16) Nedelcheva, V.; Gut, I.; Soucek, P.; Tichavska, B.; Tynkova, L.; Mraz, J.; Guengerich, F. P.; Ingelman-Sundberg, M. *Arch. Toxicol.* **1999**, *73*, 33.

(17) Sono, M.; Roach, M. P.; Coulter, E. D.; Dawson, J. H. *Chem. Rev.* **1996**, *96*, 2841.

(18) Shaik, S.; Kumar, D.; de Visser, S. P.; Altun, A.; Thiel, W. *Chem. Rev.* **2005**, *105*, 2279.

(19) (a) Rutter, R.; Hager, L. P. *J. Biol. Chem.* **1982**, *257*, 7958. (b) Hosten, C. M.; Sullivan, A. M.; Palaniappan, V.; Fitzgerald, M. M.; Terner, J. *J. Biol. Chem.* **1994**, *269*, 13966. (c) Weiss, R.; Mandon, D.; Wolter, T.; Trautwein, A. X.; Muether, M.; Bill, E.; Gold, A.; Jayaray, K.; Terner, J. *J. Biol. Inorg. Chem.* **1996**, *1*, 377. (d) Kim, S. H.; Perera, R.; Hager, L. P.; Dawson, J. H.; Hoffman, B. M. *J. Am. Chem. Soc.* **2006**, *128*, 5598.

(20) (a) Newcomb, M.; Zhang, R.; Chandrasena, R. E. P.; Halgrimson, J. A.; Horner, J. H.; Makris, T. M.; Sligar, S. G. *J. Am. Chem. Soc.* **2006**, *128*, 4580. (b) See also Jung, C.; Schünemann, V.; Lendzian, F.; Trautwein, A. X.; Contzen, J.; Galander, M.; Böttger, L. H.; Richter, M.; Barra, A.-L. *Biol. Chem.* **2005**, *386*, 1043.

(21) de Visser, S. P.; Shaik, S.; Sharma, P. K.; Kumar, D.; Thiel, W. *J. Am. Chem. Soc.* **2003**, *125*, 15779.

(22) Harris, D.; Loew, G.; Waskell, L. *J. Inorg. Biochem.* **2001**, *83*, 309.

(23) Bathelt, C. M.; Zurek, J.; Mulholland, A. J.; Harvey, J. N. *J. Am. Chem. Soc.* **2005**, *127*, 12900.

(24) Schöneboom, J. C.; Neese, F.; Thiel, W. *J. Am. Chem. Soc.* **2005**, *127*, 5840.

(25) Groves, J. T.; McClusky, G. A. *J. Am. Chem. Soc.* **1976**, *98*, 859.

(26) Newcomb, M.; Hollenberg, P. F.; Coon, M. J. *Arch. Biochem. Biophys.* **2003**, *409*, 72.

(27) Jerina, D. M.; Daly, J. W.; Witkop, B.; Zaltzman-Nirenberg, P.; Udenfriend, S. *J. Am. Chem. Soc.* **1968**, *90*, 6525.

(28) Guroff, G.; Daly, J. W.; Jerina, D. M.; Renson, J.; Witkop, B.; Udenfriend, S. *Science* **1967**, *157*, 1524.

(29) Korzekwa, K. R.; Swinney, D. C.; Trager, W. F. *Biochemistry* **1989**, *28*, 9019.

(30) Rietjens, I. M. C. M.; Soffers, A. E.; Veeger, C.; Vervoort, J. *Biochemistry* **1993**, *32*, 4801.

(31) Schröder, D.; Schwarz, H. *Helv. Chim. Acta* **1992**, *75*, 1281.

(32) Shiota, Y.; Suzuki, K.; Yoshizawa, K. *Organometallics* **2005**, *24*, 3532.

(33) See, for example, (a) Shaik, S.; Danovich, D.; Fiedler, A.; Schröder, D.; Schwarz, H. *Helv. Chim. Acta* **1995**, *78*, 1393. (b) Schröder, D.; Shaik, S.; Schwarz, H. *Acc. Chem. Res.* **2000**, *33*, 139.

(34) Korzekwa, K.; Trager, W.; Gouterman, M.; Spangler, D.; Loew, G. H. *J. Am. Chem. Soc.* **1985**, *107*, 4273.

(35) Zakharieva, O.; Grodzicki, M.; Trautwein, A. X.; Veeger, C.; Rietjens, I. M. C. M. *Biophys. Chem.* **1998**, *73*, 189.

(36) de Visser, S. P.; Shaik, S. *J. Am. Chem. Soc.* **2003**, *125*, 7413.

(37) Bathelt, C. M.; Ridder, L.; Mulholland, A. J.; Harvey, J. N. *J. Am. Chem. Soc.* **2003**, *125*, 15004.

(38) Bathelt, C. M.; Ridder, L.; Mulholland, A. J.; Harvey, J. N. *Org. Biomol. Chem.* **2004**, *2*, 2998.

(39) For a related oxidation mechanism of aromatic substrates, see (a) Hackett, J. C.; Sanan, T. T.; Hadad, C. M. *Biochemistry* **2007**, *46*, 5924.

(40) Jerina, D. M.; Daly, J. W. *Science* **1974**, *185*, 573.

(41) Koerts, J.; Soffers, A. E.; Vervoort, J.; De Jager, A.; Rietjens, I. M. C. M. *Chem. Res. Toxicol.* **1998**, *11*, 503.

(42) Williams, P. A.; Cosme, J.; Ward, A.; Angove, H. C.; Matak Vinkovic, D.; Jhoti, H. *Nature* **2003**, *424*, 464.

(43) Wester, M. R.; Yano, J. K.; Schoch, G. A.; Yang, C.; Griffin, K. J.; Stout, C. D.; Johnson, E. F. *J. Biol. Chem.* **2004**, *279*, 35630.

(44) (a) Williams, P. A.; Cosme, J.; Vinkovic, D. M.; Ward, A.; Angove, H. C.; Day, P. J.; Vonrhein, C.; Tickle, I. J.; Jhoti, H. *Science* **2004**, *305*, 683. (b) Yano, J. K.; Wester, M. R.; Schoch, G. A.; Griffin, K. J.; Stout, C. D.; Johnson, E. F. *J. Biol. Chem.* **2004**, *279*, 38091. (c) Yano, J. K.; Hsu, M. H.; Griffin, K. J.; Stout, C. D.; Johnson, E. F. *Nat. Struct. Mol. Biol.* **2005**, *12*, 822. (d) Rowland, P.; Blaney, F. E.; Smyth, M. G.; Jones, J. J.; Leydon, V. R.; Oxbrow, A. K.; Lewis, C. J.; Tennant, M. G.; Modi, S.; Eggleston, D. S.; Chenery, R. J.; Bridges, A. M. *J. Biol. Chem.* **2006**, *281*, 7614.

(45) Warshel, A.; Levitt, M. *J. Mol. Biol.* **1976**, *103*, 227.

(46) (a) Bathelt, C. M.; Mulholland, A. J.; Harvey, J. N. *Dalton Trans.* **2005**, 3470–3476. (b) Harvey, J. N.; Bathelt, C. M.; Mulholland, A. J. *J. Comput. Chem.* **2006**, *27*, 1352.

(47) See, for example, (a) Guallar, V.; Baik, M.-H.; Lippard, S. J.; Friesner, R. A. *Proc. Natl. Acad. Sci.* **2003**, *100*, 6998. (b) Schöneboom, J.; Cohen, S.; Lin, H.; Shaik, S.; Thiel, W. *J. Am. Chem. Soc.* **2004**, *126*, 4017. (c) Altun, A.; Guallar, V.; Friesner, R. A.; Shaik, S.; Thiel, W. *J. Am. Chem. Soc.* **2006**, *128*, 3924. (d) Altun, A.; Shaik, S.; Thiel, W. *J. Comput. Chem.* **2006**, *27*, 1324. (e) Zurek, J.; Foloppe, N.; Harvey, J. N.; Mulholland, A. J. *Org. Biomol. Chem.* **2006**, *4*, 3931.

(48) Bernstein, F. C.; Koetzle, T. F.; Williams, G. J. B.; Meyer, E. F.; Brice, M. D.; Rodgers, J. R.; Kennard, O.; Shimanouchi, T.; Tasumi, M. *J. Mol. Biol.* **1977**, *112*, 535.

(49) MacKerell, A. D.; Bashford, D.; Bellot, M.; Dunbrack, R. L.; Evanseck, J. D.; Field, M. J.; Fischer, S.; Gao, J.; Guo, J.; Ha, S.; Joseph-McCarthy, D.; Kuchnir, L.; Kuczera, K.; Lau, F. T. K.; Mattos, C.; Michnick, S.; Ngo, T.; Nguyen, D. T.; Prodhorn, B.; Reiher, W. E.; Roux, B.; Schlenkrich, M.; Smith, J. C.; Stote, R.; Straub, J.; Watanabe, M.; Wiorkiewicz-Kuczera, J.; Yin, D.; Karplus, M. *J. Phys. Chem. B* **1998**, *102*, 3586.

(50) Brooks, B. R.; Bruccoleri, R. E.; Olafson, B. D.; States, D. J.; Swaminathan, S.; Karplus, M. *J. Comput. Chem.* **1983**, *4*, 187.

(51) Ryckaert, J. P.; Ciccotti, G.; Berendsen, H. J. C. *J. Comp. Phys.* **1977**, *23*, 327.

(52) (a) Brooks, C. L.; Karplus, M. *J. Mol. Biol.* **1989**, *208*, 159. (b) Brooks, C. L.; Karplus, M. *J. Chem. Phys.* **1983**, *79*, 6312.

(53) Zurek, J.; Bowman, A. L.; Sokalski, W. A.; Mulholland, A. J. *Struct. Chem.* **2004**, *15*, 405.

(54) Jorgensen, W. L.; Chandrasekhar, J.; Madura, J. D. *J. Chem. Phys.* **1983**, *79*, 926.

(55) *Jaguar*, 4.2 ed.; Schrodinger, Inc.: Portland, OR, 1991−2002.

(56) Hay, J. P.; Wadt, W. R. *J. Chem. Phys.* **1985**, *82*, 299.

(57) Ponder, J. W. *TINKER:Software Tools for Molecular Design*, version 4.0; Saint Louis, MO, 2003.

(58) MacKerell, A. D.; Banavali, N.; Foloppe, N. *Biopolymers* **2000**, *56*, 257.

(59) Harvey, J. N. *Faraday Discuss.* **2004**, *127*, 165.

(60) Field, M. J.; Albe, M.; Bret, C.; Proust-De Martin, F.; Thomas, A. *J. Comput. Chem.* **2003**, *21*, 1088.

(61) Lewis, D. F. V.; Lake, B. G.; Bird, B. G.; Loizou, G. D.; Dickins, M.; Goldfarb, P. S. *Toxicol. in Vitro* **2003**, *17*, 93.

(62) Melet, A.; Assrir, N.; Jean, P.; Pilar Lopez-Garcia, M.; Marques-Soares, C.; Jaouen, M.; Dansette, P. M.; Sari, M. A.; Mansuy, D. *Arch. Biochem. Biophys.* **2003**, *409*, 80.

(63) Hammond, G. S. *J. Am. Chem. Soc.* **1955**, *77*, 334.

JP8016908